

Computationally Light Spectrally Normalized Memory Neuron Network based Estimator for GPS-denied operation of Micro-UAV

Nishanth Rao

Indian Institute of Science, Bengaluru

NISHANTHRAO@IISC.AC.IN

Suresh Sundaram

Indian Institute of Science, Bengaluru

VSSURESH@IISC.AC.IN

Varun Raghavendra

Indian Institute of Science, Bengaluru

VARUNCR@IISC.AC.IN

Abstract

This paper addresses the problem of position estimation in UAVs operating in a cluttered environment where GPS information is unavailable. A learning-based approach is proposed that takes in the rotor RPMs and past state as input and predicts the one-step-ahead position of the UAV using a novel spectral-normalized memory neural network (SN-MNN). The spectral normalization guarantees stable and reliable prediction performance. The predicted position is transformed to the global coordinate frame (GPS), which is then fused along with the odometry of other peripheral sensors like IMU, barometer, compass, etc., using the onboard extended Kalman filter (EKF) to estimate the states of the UAV. The experimental flight data collected from an RTK-GPS facility using a micro-UAV is used to train the SN-MNN. The PX4-ECL library is used to fuse the predicted data using the SN-MNN, and the estimated position is compared with actual ground truth data. The proposed algorithm doesn't require any additional onboard sensors and is computationally light. The performance of the proposed approach is compared with the current state-of-art GPS-denied algorithms, and it can be seen that the proposed algorithm has the least RMSE for position estimates.

1. Introduction

Advancements in UAV technology have enabled their widespread usage in logistic transportation, urban air mobility, and agriculture. A crucial aspect of the UAV flight is the accuracy of the onboard navigation system that provides a sense of whereabouts to the UAV controller. The onboard navigation system relies heavily on GPS sensors that accurately estimate the position of the UAV. However, in cluttered environments like forests and indoor environments, there is an intermittent loss of GPS (sometimes no GPS signal), which can lead to inaccurate position estimates, rendering the UAV unstable. Thus, it is crucial to look for GPS-denied alternatives to provide reliable position information to the UAV.

The existing literature on algorithms developed for GPS-denied operation can be broadly divided into two categories: algorithms that use reliable position estimates generated by either vision-based systems or simultaneous localization and mapping (SLAM)-based systems. In (Mohta et al., 2018), stereo camera-based localization is employed for fast and agile navigation of the UAV in the presence of surrounding obstacles. In (Mebarki and Lippiello, 2014), the concept of *image moments* is utilized from environment images to estimate the translational velocity of the UAV reliably. A combination of optical flow and ultrasound sensors has been used in (Tsai and Zhuang, 2016) to

achieve a stable indoor hovering performance of a micro aerial vehicle. However, vision-based localization systems fail to provide reliable odometry in varying lighting conditions and exhibit drift when no features are available to track. Further, one needs to tune the parameters meticulously to achieve reliable performance in a known environment (Balamurugan et al., 2016).

On the other hand, SLAM-based methods mostly require LiDAR sensors or compatible vision-based sensors. In (Kim et al., 2005), a 6-DOF SLAM is proposed that builds a relative map from surrounding features and provides odometry measurements relative to this map. In (Urzua et al., 2017), a vision-based SLAM algorithm is employed using a monocular camera and an ultrasound camera for navigation. To alleviate the problems specific to vision-based sensors, (Khattak et al., 2019) employs an infrared thermal sensor to obtain localization information in the presence of dark, texture-less environments with dust-filled / smoke-filled settings. However, SLAM-based methods work efficiently only in a cluttered environment with some external objects that can be tracked throughout the flight. When flying in areas without any surrounding objects or in fast dynamic environments, vision-based odometry and SLAM-based methods fail to provide accurate position estimates to the UAV. Reliable vision-based odometry systems require high FPS performance cameras that are prohibitively expensive. Moreover, these methods require additional onboard specialized sensors that can be limiting in a micro-UAV setting and tend to consume extra power that can limit the overall endurance of the UAV.

In this paper, a *data-driven model learning*-based approach is proposed to estimate the UAV position using a Spectrally Normalized Memory Neuron Network (SN-MNN) that is invariant to the environmental features and external factors like surrounding objects, varying lighting conditions, etc. The SN-MNN predicts the position of the UAV based on the rotor RPM input and previous UAV states. It is shown theoretically that spectral normalization guarantees a stable prediction performance by constraining the Lipschitz constant of the fitted function. The look-ahead predicted position is transformed to a global coordinate (GPS), and extended Kalman filter-based state fusion is used to estimate the UAV states. The experimental flight data from an RTK-GPS facility is used for training the SN-MNN. The model learning-based approach is validated using the PX4-ECL library on sample test flights. Finally, the performance of the proposed algorithm is compared with other state-of-art GPS-denied algorithms. It can be seen that the proposed algorithm has the least RMSE in predicting the position of the UAV in comparison to other techniques.

2. Spectral-Normalized Memory Neuron Network-based State Estimation

First, this section presents the UAV dynamic equations and input-output model. Next, the novel data-driven spectrally normalized memory neuron network is presented to predict the position of the UAV from the past state and current input. Finally, the predicted local position is converted to global coordinates (GPS) and state fusion is carried out to estimate the UAV states.

2.1. Input-Output Model of UAV

The physics-based mathematical model of a typical UAV system is given below:

$$\begin{aligned} \dot{\mathbf{x}} &= \mathbf{v}, \quad m\dot{\mathbf{v}} = mg\hat{\mathbf{k}} + \mathbf{R}\hat{\mathbf{k}}f_t + \tilde{\mathbf{f}} & (1a) \\ \dot{\mathbf{R}} &= \mathbf{R}\boldsymbol{\Omega}^\times, \quad \mathbf{J}\dot{\boldsymbol{\Omega}} + \boldsymbol{\Omega}^\times\mathbf{J}\boldsymbol{\Omega} = \boldsymbol{\tau} + \tilde{\boldsymbol{\tau}} & (1b) \\ \text{with, } f_t &= K_\omega (\omega_1^2 + \omega_2^2 + \omega_3^2 + \omega_4^2) & (1c) \\ \boldsymbol{\tau} &= \begin{bmatrix} \tau_x \\ \tau_y \\ \tau_z \end{bmatrix} = \begin{bmatrix} K_\omega l (\omega_3^2 - \omega_1^2) \\ K_\omega l (\omega_4^2 - \omega_2^2) \\ K_d (\omega_2^2 + \omega_4^2 - \omega_1^2 - \omega_3^2) \end{bmatrix} & (1d) \end{aligned}$$

where $\hat{\mathbf{k}} = [0 \ 0 \ 1]^T$ is the unit vector along the z -axis, $\mathbf{x} \in \mathbb{R}^3$ is the position of the UAV with mass $m \in \mathbb{R}$ and moment of inertia $\mathbf{J} \in \mathbb{R}^{3 \times 3}$, $\mathbf{v} \in \mathbb{R}^3$ is the linear velocity, $\mathbf{R} \in \mathbb{R}^{3 \times 3}$ is the rotation matrix that converts a vector from the UAV-fixed body frame to the inertial frame, $\boldsymbol{\Omega} \in \mathbb{R}^3$ is the angular velocity of the UAV, $f_t \in \mathbb{R}$ is the input thrust vector and $\boldsymbol{\tau} \in \mathbb{R}^3$ is the input torque vector given by Eq. (1c) and (1d) respectively. The quantities ω_i denotes the rotational velocity of the i^{th} motor in (rad/s), l denotes the arm length of the UAV, and the constants K_ω, K_d denote the motor constant and the drag coefficient respectively. The operator $(\cdot)^\times : \mathbb{R}^3 \rightarrow \mathbb{R}^{3 \times 3}$ is the hat operator that converts a vector to a skew-symmetric matrix. The quantities $\tilde{\mathbf{f}}, \tilde{\boldsymbol{\tau}}$ represent the external complex aerodynamic forces and torques on the UAV that are mostly unknown or cannot be analytically modelled. In real world, the dynamics given by Eq. (1) are rudimentary and cannot be relied upon for estimating the UAV states due to presence of noise, model uncertainties and external disturbances.

In general, one can use *billings theorem* (Leontaritis and Billings, 1985) to write the input-output model of a dynamical system as:

$$\mathbf{y}_{k+1} = f(\mathbf{y}_k, \dots, \mathbf{y}_{k-n}, \mathbf{u}_k, \dots, \mathbf{u}_{k-n}) \quad (2)$$

where $f(\cdot)$ is an unknown nonlinear function, n is the order of the system, \mathbf{y}_k and \mathbf{u}_k is the output of and input to the system respectively at time step k . Note that one can use a recurrent neural network to approximate the unknown nonlinear function using the current input and past output. It has been shown in the literature that the *Memory Neuron Network* (MNN) Sastry et al. (1994) is more efficient in approximating the dynamics accurately than other state-of-the-art recurrent neural networks (Rao and Sundaram, 2021). The presence of uncertainty in thrust and the unknown disturbance influences the stability/reliability of prediction. The next section proposes a spectrally normalized MNN to learn the UAV model accurately.

2.2. Spectral-Normalized Memory Neural Network based Model Learning

The Spectrally Normalized Memory Neural Network (SN-MNN) contains *fully connected* network neurons (white circle) with its associated memory neurons (black solid circle). The unique nature of the connection between the Network Neurons and the Memory Neurons (see Fig.1) makes the network *recurrent* in nature. The network is parameterized by $\boldsymbol{\theta} = \{({}^1\mathbf{W}, {}^1\mathbf{Q}), \dots, ({}^L\mathbf{W}, {}^L\mathbf{Q})\}$, the weights corresponding to both the network neurons (\mathbf{W}) as well as the memory neurons (\mathbf{Q}). The left superscript denotes the layer number. Thus, the output of SN-MNN to an input \mathbf{p} can be

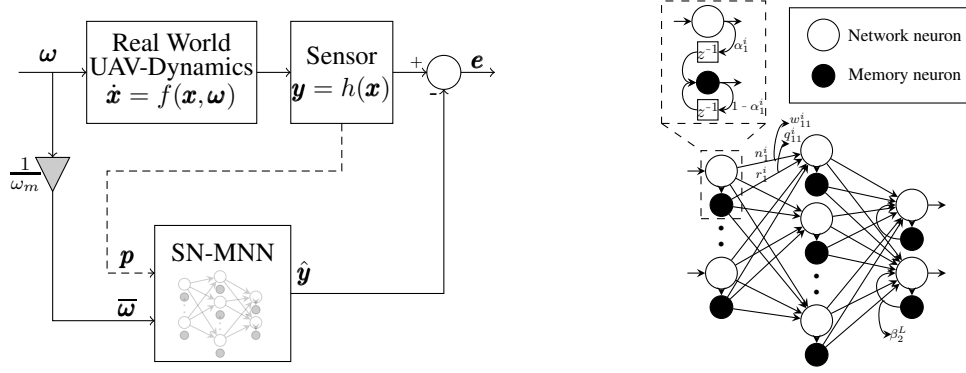


Figure 1: Figure on the left shows a schematic block diagram of SN-MNN training. The error is used for backpropagation. The motor input ω is normalized by the maximum rotor speed ω_m before feeding to the SN-MNN. The figure on the right shows the schematic diagram of a fully connected SN-MNN consisting of a single hidden layer.

compactly represented as:

$$f(\mathbf{p}, \boldsymbol{\theta}) = {}^L \mathbf{W} (\dots \phi({}^2 \mathbf{W} (\phi({}^1 \mathbf{W} \mathbf{p} + {}^1 \mathbf{Q}^1 \mathbf{r})) + {}^2 \mathbf{Q}^2 \mathbf{r}) \dots) + {}^L \mathbf{Q}^L \mathbf{r} \quad (3)$$

where $\phi(\cdot)$ denotes the activation function and ${}^l \mathbf{r}$ denotes the output of the memory neurons present in the l^{th} layer. The recurrence relationship between the memory neurons and the network neurons can be represented as:

$${}^l \mathbf{r}_k = {}^l \boldsymbol{\alpha}^l \mathbf{n}_{k-1} + (1 - {}^l \boldsymbol{\alpha}^l) {}^l \mathbf{r}_{k-1} \quad (4)$$

where ${}^l \mathbf{n} = \phi(\cdot)$ is the output of the activation function in the l^{th} layer and ${}^l \boldsymbol{\alpha}$ is the weight of the feedback connections between the network and the memory neurons in the l^{th} layer (see Fig. 1).

The Lipschitz constant γ of a real valued function $f: \mathbb{R}^n \rightarrow \mathbb{R}$ is defined mathematically as:

$$\|f(\mathbf{p}_2) - f(\mathbf{p}_1)\|_2 \leq \gamma \|\mathbf{p}_2 - \mathbf{p}_1\|_2 \quad (5)$$

The Lipschitz constant of a differentiable function is the *maximum spectral norm* of its Jacobian over the function's domain: $\gamma = \sup_{\mathbf{p}} \rho(\nabla f(\mathbf{p}))$, where $\rho(\mathbf{A})$ denotes the spectral norm of the matrix \mathbf{A} which is defined as the square root of maximum eigenvalue of the matrix $\mathbf{A}^H \mathbf{A}$. As demonstrated in (Shi et al., 2019), it is essential to limit the Lipschitz constant of a neural network to ensure stable reliable prediction performance that is comparable with the actual dynamics of the UAV. The following Theorem guarantees the Lipschitz constant of the SN-MNN:

Theorem 1 *The Lipschitz constant of the entire spectrally normalized memory neuron network satisfies the inequality $\|f(\mathbf{p}, \boldsymbol{\theta})\|_2 \leq \gamma$ under the spectral weight normalization:*

$$\overline{\mathbf{W}} = \left(\frac{\mathbf{W}}{\rho(\mathbf{W})} \right) \cdot \gamma^{\frac{1}{L}}, \quad \overline{\mathbf{Q}} = \left(\frac{\mathbf{Q}}{\rho(\mathbf{Q})} \right) \cdot \gamma^{\frac{1}{L}} \quad (6)$$

with γ being the intended Lipschitz constant of the network, and $\tanh(\cdot)$ as the activation function.

Proof The spectral norm of a linear map $g(\mathbf{p}) = \mathbf{W}\mathbf{p} + \mathbf{b}$ can be simplified as: $\sup_{\mathbf{p}} \rho(\nabla g) = \sup_{\mathbf{p}} \rho(\mathbf{W}) = \rho(\mathbf{W})$. Moreover, using the inequality $\text{Lip}(g_1 \circ g_2) \leq \text{Lip}(g_1) \cdot \text{Lip}(g_2)$ and the fact that $\text{Lip}(\tanh(\cdot)) = 1$ along with Eq. (3) leads to:

$$\|f(\mathbf{p}, \boldsymbol{\theta})\|_2 = \text{Lip} \left({}^L \overline{\mathbf{W}} \cdot \left(\dots \phi \left({}^2 \overline{\mathbf{W}} \cdot \left(\phi \left({}^1 \overline{\mathbf{W}} \mathbf{p} + {}^1 \overline{\mathbf{Q}} \mathbf{r} \right) + {}^2 \overline{\mathbf{Q}} \mathbf{r} \right) \dots \right) + {}^L \overline{\mathbf{Q}} \mathbf{r} \right) \quad (7)$$

$$\leq \prod_{l=1}^L \rho({}^l \overline{\mathbf{W}}) = \prod_{l=1}^L \gamma^{\frac{1}{L}} = \gamma \quad (8)$$

Here, the term ${}^i \overline{\mathbf{Q}} \mathbf{r}$ can be considered as a "time-varying" bias that is independent of input \mathbf{p}_k at current time step k , and thus, doesn't affect the Lipschitz constant. However, the term \mathbf{r} depends on \mathbf{p}_{k-1} through Eq. 4 which is why the weight matrix \mathbf{Q} corresponding to the memory neurons must also undergo spectral normalization. ■

For training the network, the *modified backpropagation* approach as described in (Sastry et al., 1994) is used, with the following cost function being minimized during training at every time step:

$$\boldsymbol{\theta}^* = \underset{\boldsymbol{\theta}}{\text{argmin}} \sum_{k=1}^N \frac{1}{T} \|\mathbf{y}_k - f(\mathbf{p}_k, \boldsymbol{\theta})\|_2^2 \quad (9a)$$

$$\text{such that, } \|f(\mathbf{p}_k, \boldsymbol{\theta})\|_2 \leq \gamma \quad (9b)$$

where the input $\mathbf{p}_k = [\mathbf{y}_{k-1}^T \ \overline{\boldsymbol{\omega}}_k^T \ \boldsymbol{\Theta}_k^T]^T$ consists of the previous position of the UAV $\mathbf{y}_{k-1} \in \mathbb{R}^3$, the roll-pitch-yaw orientation of the UAV $\boldsymbol{\Theta}_k \in \mathbb{R}^3$ and the current normalized motor RPM $\overline{\boldsymbol{\omega}}_k \in \mathbb{R}^4$. The training process of the network is illustrated in Fig. 1. Let \mathbf{e} be the error vector. Due to the constraint of Eq. (9b), the update rules for \mathbf{W} and \mathbf{Q} are as follows:

$${}^l \mathbf{W}_{k+1} = \frac{\gamma^{\frac{1}{L}}}{\rho({}^l \mathbf{W}_k)} \left({}^l \mathbf{W}_k - \eta \cdot {}^l \mathbf{n}_k \mathbf{e}^T \right) \quad (10)$$

$${}^l \mathbf{Q}_{k+1} = \frac{\gamma^{\frac{1}{L}}}{\rho({}^l \mathbf{Q}_k)} \left({}^l \mathbf{Q}_k - \eta \cdot {}^l \mathbf{r}_k \mathbf{e}^T \right) \quad (11)$$

More details of the update rule derivation are provided in the supplementary material Rao (2022).

2.3. GPS Conversion and State Estimation

The network predicts the position of the UAV based on the rotor RPM input. This position estimate can be used during *state fusion* typically performed by an onboard Extended Kalman Filter (EKF), in addition to the state information provided by other peripheral sensors like IMU, compass, magnetometer, airflow sensor etc. In this work, the position estimates given by the network are converted to *GPS coordinates* $\boldsymbol{\zeta}_k$, also known as geodetic coordinates (latitude ϕ , longitude λ , altitude z) and transformed GPS coordinates are used by the EKF for state estimation. This is illustrated in Fig. 2 and Fig. 3. Since many flight controllers offer out-of-box support for real-time GPS fusion, it has been adopted in this paper. Moreover, ground control software utilises GPS coordinates to visualise the UAV path and monitor its itinerary and the course of navigation.

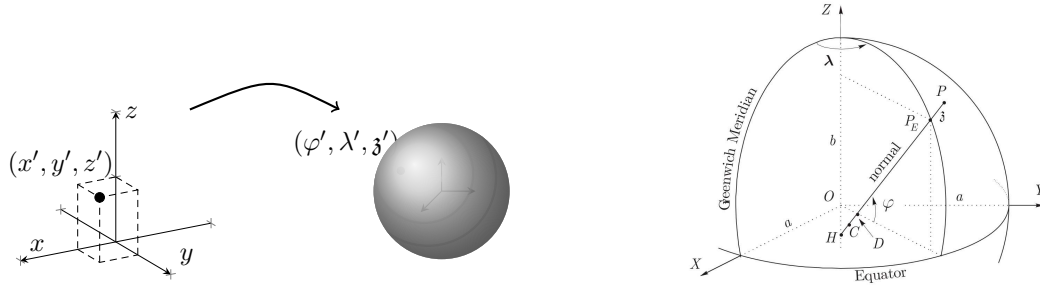


Figure 2: Figure on the left shows the GPS Conversion from East-North-Up (ENU) coordinate vector $\mathbf{x} = (x', y', z')$ shown in to geodetic (latitude, longitude and altitude) coordinate vector $\boldsymbol{\zeta} = (\varphi', \lambda', \mathfrak{z}')$. Figure on the right shows the ECEF coordinate system and the geodetic coordinate system together.

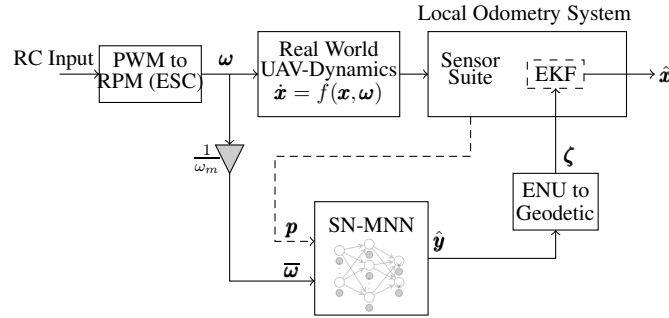


Figure 3: Figure illustrates the state fusion replay process. Based on the RPM input, the orientation of the UAV, and the previous position of the UAV, the trained SN-MNN predicts the position of the UAV, which is provided to the onboard EKF as GPS coordinates. The Sensor suite consists of peripheral sensors like IMU, compass, magnetometer etc., and the state fusion process is performed by the EKF.

The ENU coordinates must first be converted to the ECEF (Earth-Center, Earth-Fixed) coordinate system before converting it to the GPS coordinates. Detailed information on converting the ENU coordinates to the GPS coordinates (via ECEF coordinates) is provided in the supplementary material [Rao \(2022\)](#). However, the following equations summarize the conversion to GPS coordinates:

$$\left[\varphi = 2 \tan^{-1} \left(\frac{Z}{D + \sqrt{D^2 + Z^2}} \right); \lambda = 2 \tan^{-1} \left(\frac{Y}{X + \sqrt{X^2 + Y^2}} \right); \mathfrak{z} = \frac{\kappa + e^2 - 1}{\kappa} \left(\sqrt{D^2 + Z^2} \right) \right] \quad (12)$$

where the parameters κ and D can be calculated by the set of equations given in the supplementary material [Rao \(2022\)](#). This process is briefly summarized in Fig. 3.



Figure 4: Figure on the left shows a snapshot of the UAV flight while collecting data. Figure on the right shows a snapshot of the RTK-GPS facility.

3. Experimental Results

First, this section presents the RTK GPS setup and the micro-UAV hardware configuration. Next, the experimental flight data collection for training the SN-MNN is discussed. Finally, the performance of SN-MNN prediction, flight evaluation and comparative study results are presented.

3.1. RTK GPS setup and UAV hardware

The experimental setup consists of an outdoor RTK GPS facility (Here+ RTK Base with Here3 RTK GPS) with base station survey-in accuracy of 1m (relative accuracy of 10cm) and a custom-built micro-UAV (generic 250 racer frame) with the Pixhawk 4 Flight Controller that runs on PX4 firmware. The RTK facility and a micro-UAV operating in the facility are shown in Fig. 4. The drone weighs about 1.1 Kg, with a RaspberryPi 4 onboard computer. The onboard sensors include an accelerometer, gyroscope, barometer and a compass, all present inside the flight controller. In addition to this, the Velox V2 1950KV T-motors are used with a 5-inch 3 blade propeller configuration. The data is collected on a typical day with mild steady wind influences.

3.2. Experimental Flight Data Collection and Processing

For training the network, experimental data is collected from the test facility. The states of the UAV and the 4 rotor rpm are logged for multiple flights. The DShot protocol is used by the F55A electronic speed controller (ESC), which measures the rotor RPM values based on the back-EMF from the motor. The flight data mainly consists of random trajectories performed manually and certain square and circular trajectories performed autonomously by the UAV. These flights ensure that all possible UAV configuration in its state-space are captured.

Next, a common *sampling frequency* is chosen to sample the data corresponding to different sensors (IMU, Barometer, Compass, RPM data and the RTK GPS position information). The RPM values are normalized based on the motor's maximum RPM. The final data consists of 12 columns: one common timestamp for all other columns, 4 normalized rotor rpm (from ESC), position, and

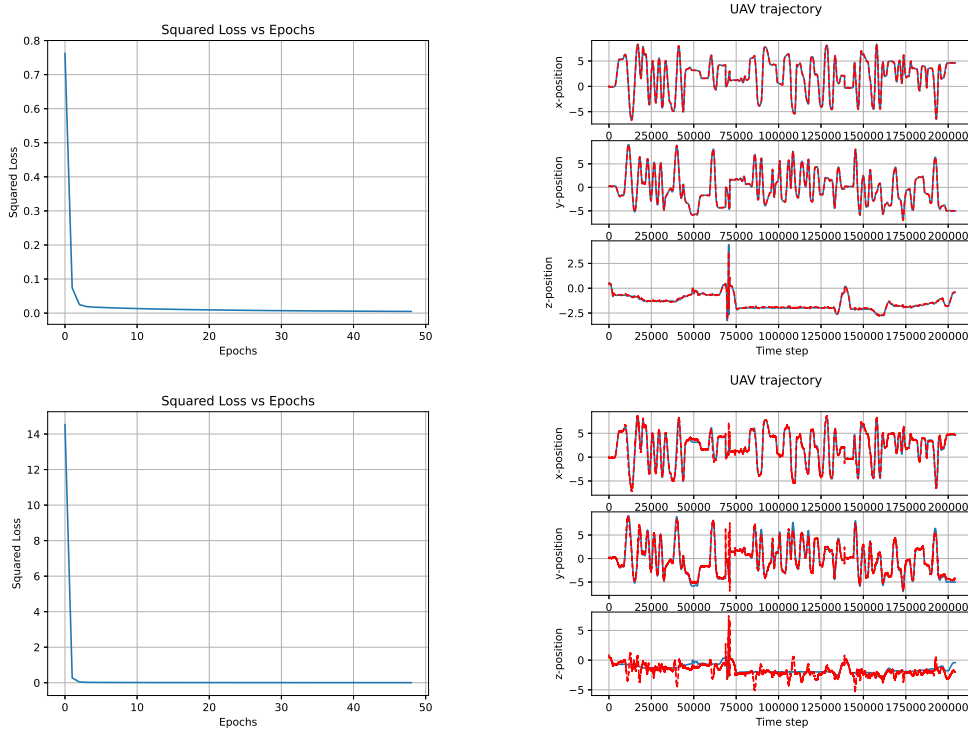


Figure 5: Figure on the left shows the variation of the training loss vs epoch number. Figure on the right shows the prediction of the SN-MNN for the entire testing data set. The figures in the second row shows the performance of the network without spectral normalization.

quaternion orientation of the UAV. The entire data is then split into training and testing data in the ratio of 3:2.

3.3. SN-MNN Prediction Performance Evaluation

The SN-MNN is trained to predict the one-step-ahead position of the UAV, with the current UAV position $\mathbf{y}_k \in \mathbb{R}^3$, orientation (Euler angles) $\mathbf{q}_k \in \mathbb{R}^4$ and the normalized rotor RPM $\bar{\omega}_k \in \mathbb{R}^4$ as the input to the network. Hence, the selected architecture of SN-MNN is: 11 input neurons, 100 hidden neurons and 3 output neurons. The network neurons in the hidden layer uses $\tanh(\cdot)$ activation and the network neurons in output layer employ linear activation function. The network is implemented in Python using Numpy Library. The network is trained for a total of 50 epochs. The variation of the squared loss during training is shown in Fig. 5 for with and without spectral normalization.

The output of the network for the entire test data (combined into one) is shown in Fig. 5. The RMSE for the entire position prediction is about $5.84cm$, whereas, for the network without spectral normalization, the RMSE error is about $50cm$, thus justifying the requirement for a spectrally normalized network. It can be seen from Fig. 5 that the network has successfully learned the UAV dynamics accurately. The value of the Lipschitz constant γ (here $\gamma = 1$) of the network plays an important role in the stabilization of the network during the training process. It also determines "how fast" the network output can vary: For e.g. if the UAV is mostly hovering and making slow move-

ments, the Lipschitz constant can be set to a low value. If the UAV is performing aggressive sharp maneuvers frequently, then the Lipschitz constant of the network must be set to a high value. In this paper, the trajectory data is collected for a UAV that mostly cruises and exhibits slow maneuvers.

3.4. State Fusion and Experimental data evaluation

Once the predicted position \mathbf{y}_k is obtained from the SN-MNN, the GPS geodetic vector ζ_k is calculated from Eq. 12, which is then given to the EKF for state fusion along with other state information like orientation, linear velocities (IMU) and UAV heading (compass). This is illustrated in Fig. 3. An instance of the PX4-ECL library is started on the onboard Raspberry-pi computer, and the state estimation process using the position predicted by the SN-MNN starts parallelly with the state-estimation process on the PX4-Autopilot that uses the GPS for the UAV flight. This is done to facilitate a real-time comparison of the position obtained (after state fusion) from the proposed algorithm vs. the position obtained (after state fusion) using an RTK GPS.

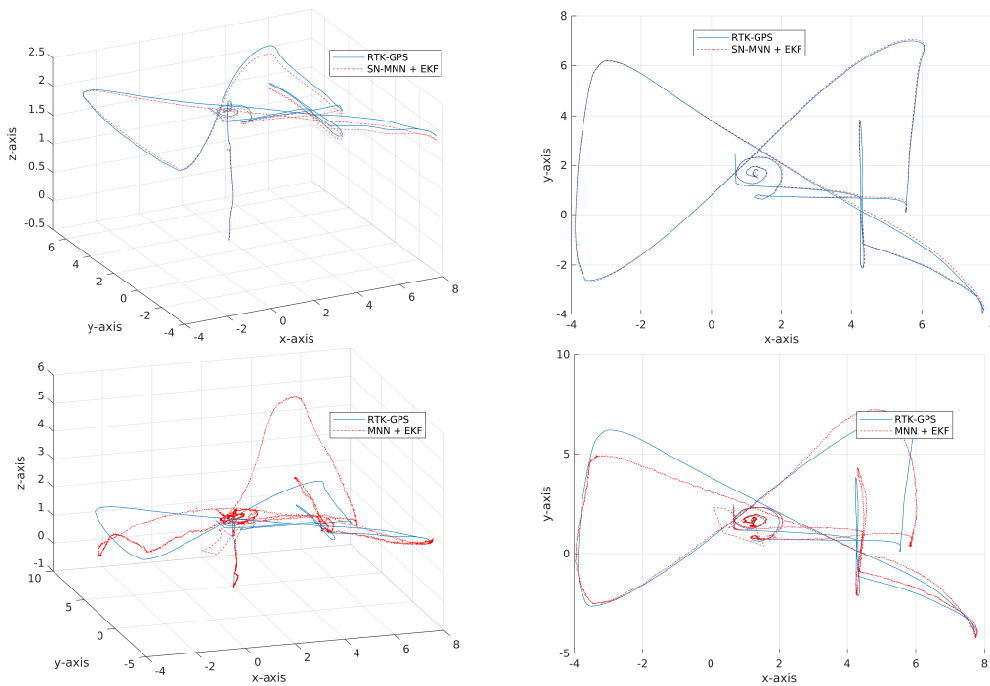


Figure 6: Figures illustrate the performance of the proposed algorithm with and without *spectral normalization* for the first sample test trajectory. For convenience, the top views are shown on the right, corresponding to their 3D trajectories. The second-row figures show the performance without the spectral normalization process.

Table 1: RMSE comparison

	VINS-Mono	VIO	MNN + EKF	SN-MNN + EKF
RMSE (m)	0.18	0.13	0.542	0.05953

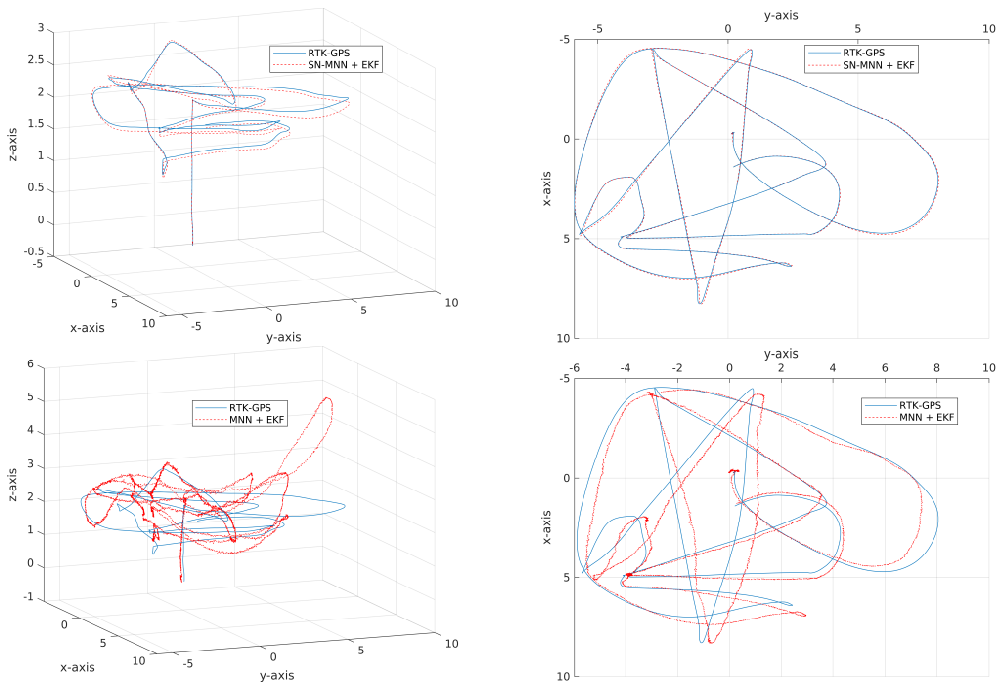


Figure 7: Figures illustrate the performance of the proposed algorithm with and without *spectral normalization* for the second sample test trajectory. For convenience, the top views are shown on the right, corresponding to their 3D trajectories. The second-row figures show the performance without the spectral normalization process.

The outputs for two sample test trajectories are shown in Fig. 6 and Fig. 7 after the PX4-ECL state fusion is performed. It must be noted that the GPS fusion only affects the position and linear velocity of the UAV, not its rotational components. The RMSE between the estimated positions and the actual positions of the UAV for the course of the entire test flight duration (all test trajectories combined) is around $6cm$, whereas, for the network without spectral normalization, the RMSE is around $55cm$. Further, Table 1 shows a comparison with two state-of-art methods, namely the Visual Inertial Navigation System (VINS) and the Visual Inertial Odometry (VIO). The RMSE reported by these methods is compared along with the proposed method in this work. It can be seen that the RMSE reduces by about 60% for VINS-mono(Qin et al., 2018) and about 40% for VIO(Loianno et al., 2016). Further, the algorithm is computationally light, as one has to implement only the trained feedforward SN-MNN model. This implementation can be done directly on the flight controller, requiring no additional onboard computer. Thus, from the above results, it can be concluded that the proposed algorithm can be used to estimate the UAV states from the rotor RPM reliably.

References

Mohammad K Al-Sharman, Yahya Zweiri, Mohammad Abdel Kareem Jaradat, Raghad Al-Husari, Dongming Gan, and Lakmal D Seneviratne. Deep-learning-based neural network training for

- state estimation enhancement: Application to attitude estimation. *IEEE Transactions on Instrumentation and Measurement*, 69(1):24–34, 2019.
- Ammar Assad, Wassim Khalaf, and Ibrahim Chouaib. Radial basis function kalman filter for attitude estimation in GPS-denied environment. *IET Radar, Sonar & Navigation*, 14(5):736–746, 2020.
- G Balamurugan, J Valarmathi, and VPS Naidu. Survey on uav navigation in gps denied environments. In *2016 International conference on signal processing, communication, power and embedded system (SCOPES)*, pages 198–204. IEEE, 2016.
- Christian Forster, Deon Sabatta, Roland Siegwart, and Davide Scaramuzza. RFID-based hybrid metric-topological slam for GPS-denied environments. In *2013 IEEE International Conference on Robotics and Automation*, pages 5228–5234. IEEE, 2013.
- Geodetic System. Geodetic system — the GIS encyclopedia, 2017. URL http://wiki.gis.com/wiki/index.php/Geodetic_system. [Online; modified 13-February-2017].
- Charles Karney. Geographiclib. *online at http://geographiclib.sourceforge.net*, 2015.
- Shehryar Khattak, Frank Mascarich, Tung Dang, Christos Papachristos, and Kostas Alexis. Robust thermal-inertial localization for aerial robots: A case for direct methods. In *2019 International Conference on Unmanned Aircraft Systems (ICUAS)*, pages 1061–1068. IEEE, 2019.
- Jonghyuk Kim, Salah Sukkarieh, et al. 6dof slam aided GNSS/INS navigation in GNSS denied and unknown environments. *Positioning*, 1(09), 2005.
- IJ Leontaritis and Stephen A Billings. Input-output parametric models for non-linear systems part i: deterministic non-linear systems. *International journal of control*, 41(2):303–328, 1985.
- Colton Lindstrom, Randall Christensen, and Jacob Gunther. An investigation of GPS-denied navigation using airborne radar telemetry. In *2020 IEEE/ION Position, Location and Navigation Symposium (PLANS)*, pages 168–176, 2020.
- Giuseppe Loianno, Michael Watterson, and Vijay Kumar. Visual inertial odometry for quadrotors on se (3). In *2016 IEEE International Conference on Robotics and Automation (ICRA)*, pages 1544–1551. IEEE, 2016.
- Andr as L Majdik, Damiano Verda, Yves Albers-Schoenberg, and Davide Scaramuzza. Air-ground matching: Appearance-based GPS-denied urban localization of micro aerial vehicles. *Journal of Field Robotics*, 32(7):1015–1039, 2015.
- Rafik Mebarki and Vincenzo Lippiello. Image moments-based velocity estimation of UAVs in GPS denied environments. In *2014 IEEE International Symposium on Safety, Security, and Rescue Robotics (2014)*, pages 1–6. IEEE, 2014.
- Kartik Mohta, Michael Watterson, Yash Mulgaonkar, Sikang Liu, Chao Qu, Anurag Makineni, Kelsey Saulnier, Ke Sun, Alex Zhu, Jeffrey Delmerico, et al. Fast, autonomous flight in GPS-denied and cluttered environments. *Journal of Field Robotics*, 35(1):101–120, 2018.

Tong Qin, Peiliang Li, and Shaojie Shen. Vins-mono: A robust and versatile monocular visual-inertial state estimator. *IEEE Transactions on Robotics*, 34(4):1004–1020, 2018. doi: 10.1109/TRO.2018.2853729.

Nishanth Rao. Supplementary Material for this paper. https://drive.google.com/drive/folders/1JhRFm5EMxU0DQkKRFG7VsiZ9myiokVK_?usp=s 2022. [Online Google drive].

Nishanth Rao and Suresh Sundaram. Spatio-temporal look-ahead trajectory prediction using memory neural network. In *2021 International Joint Conference on Neural Networks (IJCNN)*, pages 1–8, 2021. doi: 10.1109/IJCNN52387.2021.9534209.

Paul Riseborough and Team. PX4 Estimation and Control Library. <https://github.com/PX4/PX4-ECL>, 2016.

PS Sastry, G Santharam, and KP Unnikrishnan. Memory neuron networks for identification and control of dynamical systems. *IEEE transactions on neural networks*, 5(2):306–319, 1994.

Davide Scaramuzza, Michael C Achtelik, Lefteris Doitsidis, Fraundorfer Friedrich, Elias Kosmatopoulos, Agostino Martinelli, Markus W Achtelik, Margarita Chli, Savvas Chatzichristofis, Laurent Kneip, et al. Vision-controlled micro flying robots: from system design to autonomous navigation and mapping in GPS-denied environments. *IEEE Robotics & Automation Magazine*, 21(3):26–40, 2014.

Guanya Shi, Xichen Shi, Michael O’Connell, Rose Yu, Kamyar Azizzadenesheli, Animashree Anandkumar, Yisong Yue, and Soon-Jo Chung. Neural lander: Stable drone landing control using learned dynamics. In *2019 International Conference on Robotics and Automation (ICRA)*, pages 9784–9790. IEEE, 2019.

Shang-En Tsai and Shih-Hsien Zhuang. Optical flow sensor integrated navigation system for quadrotor in GPS-denied environment. In *2016 International Conference on Robotics and Automation Engineering (ICRAE)*, pages 87–91. IEEE, 2016.

Sarquis Urzua, Rodrigo Munguía, and Antoni Grau. Vision-based slam system for MAVs in GPS-denied environments. *International Journal of Micro Air Vehicles*, 9(4):283–296, 2017.

Hugues Vermeille. Direct transformation from geocentric coordinates to geodetic coordinates. *Journal of Geodesy*, 76(8):451–454, 2002.

Hugues Vermeille. An analytical method to transform geocentric into geodetic coordinates. *Journal of Geodesy*, 85(2):105–117, 2011.

Shady Zahran, Adel Moussa, and Naser El-Sheimy. Enhanced drone navigation in GNSS denied environment using VDM and hall effect sensor. *ISPRS International Journal of Geo-Information*, 8(4):169, 2019.

Kai Zhu, Xuan Guo, Changhui Jiang, Yujingyang Xue, Yuanjun Li, Lin Han, and Yuwei Chen. MIMU/odometer fusion with state constraints for vehicle positioning during beidou signal outage: Testing and results. *Sensors*, 20(8):2302, 2020.